Distribution of Star-Branched Random-Flight Chains in Solution near a Plane Barrier

Edward F. Casassa

Department of Chemistry, Carnegie Mellon University, Pittsburgh, Pennsylvania 15213

Received April 5, 1995; Revised Manuscript Received August 7, 1995[⊗]

ABSTRACT: Equilibrium distributions of polymer chain segments in solution near an impenetrable, but otherwise noninteracting, plane barrier are studied for random-flight regular star species comprising identical linear subchains joined at a common node. Although the polymer concentration in the diffuse depletion layer created by entropic repulsion of chains from the barrier vanishes at the wall, segments in different positions in the chains are not distributed identically. Chain ends are favored over interior segments near the wall, and branch nodes experience the greatest repulsion. Calculations of segment density versus distance profiles for any given position in the chain and the overall averaged density profile require single and double numerical integration, respectively, but certain analytic properties of the profiles can be derived. Correlation with the mean projection of the polymer molecule on a line is of particular interest since this quantity is a measure of the mean thickness of the depletion layer for any molecular model without molecular interactions.

Introduction: Basic Relations

It has been recognized, at least since 1954, that the diminished conformational freedom of flexible polymer chains in a solution in contact with an impenetrable but otherwise passive interface must produce an entropically unfavorable environment from which chain segments are repelled.[1] This effect is manifested by a diffuse equilibrium "depletion layer" at the boundary. Long ago, with Y. Tagami, we applied random-flight chain statistics within geometrically simple cavities to fashion a quantitative theory of the separation of polymers in size-exclusion chromatography in terms of the entropic repulsion.[2] Although the pertinent mathematical apparatus was worked out in ref 2 for both linear and star-shaped branched chains, we did not in that work consider explicitly the distribution of polymer in the depletion layer. In a later study[3] we did discuss in detail the distribution of random-flight linear chains near a plane boundary; and in a more recent collaboration[4] we utilized the distribution of random flights within a spherical cavity to interpret neutron scattering data from latex particles containing high molecular weight polymer. One reason for the growth of interest in the structure of depletion layers is the improvement of optical techniques for studying the range of dimensions involved. For instance, with high molecular weight polymers, depletion layers and adsorption layers can be studied by evanescent-wave induced fluorescence with radiation ranging from visible to X-ray wavelengths.[5-7] Another focus of interest is the effect of entropic repulsion on the stability of a colloid suspended in a polymer solution.[8]

In this paper, we go beyond the study of linear random-flight chains presented in ref 3 to deal with depletion layers for model branched chains of "regular star" type near a plane barrier. An f-arm regular star comprises f identical linear subchains of n statistical segments joined at one end to a common node. We enumerate the segments from the node out to segment n at the free end of the subchain.

Two simple, related random-flight probabilities for linear chains, given by eqs 1 and 2 below, can be combined to develop all the expressions we will need. The probability that a random flight started from a point at distance x from the wall ends after n steps within an increment dx' at a distance x' from the wall, without touching it (i.e., the probability of success in generating such a configuration), is:

$$P_n(x'|x)\,dx' = \frac{A}{\pi^{1/2}}[e^{-A^2(x'-x)^2} - e^{-A^2(x'+x)^2}]\,dx' \quad (1)$$

with $A = (3/2nb^2)^{1/2}$, b denoting the root-mean-square step length.[9,10] By integrating over all destinations x', we get the probability that any random-flight configuration of n steps generated from x is successful:

$$P_n(x) = \int_0^\infty P_n(x'|x)\,dx' = \mathrm{erf}(Ax) \quad (2)$$

where erf denotes the error function:

$$\mathrm{erf}(y) = \frac{2}{\pi^{1/2}}\int_0^y e^{-v^2}\,dv \quad (3)$$

Since $P_n(x)$ is the fraction of random configurations of n steps generated from x that are successful, it also represents the equilibrium number density of linear chain ends in a population at x, relative to unit density in the bulk solution phase far from the wall, where chain configurations are unconstrained.

To deal with star molecules, we first suppose that a branch node is put at position x. To produce the star, we generate independently f identical subchains beginning at x. The probability of success is $[P_n(x)]^f$, which thus represents the relative density of star nodes at x in a population of f-arm stars. At this stage it is convenient to introduce dimensionless distance variables $t = Ax$ and $t' = Ax'$. Then the relative equilibrium density of star nodes as a function of distance from the wall is given by

$$\rho_0(t) = [\mathrm{erf}(t)]^f \quad (4)$$

To obtain the density profile $\rho_n(t)$ for free ends (segment n) of star molecules, we can visualize generating a linear chain that begins at x and reaches x', and also generating $f - 1$ identical chains at x' to obtain the

[⊗] Abstract published in *Advance ACS Abstracts,* October 15, 1995.

0024-9297/95/2228-7756$09.00/0

joint probability $[P_n(x')]^{f-1}P_n(x'|x)$. Integration over x'- (or t') then yields the concentration profile for a population of end segments:

$$\rho_n(t) = \int_0^\infty [\mathrm{erf}(t')]^{f-1} \frac{1}{\pi^{1/2}} [e^{-(t'-t)^2} - e^{-(t'+t)^2}]\, dt' \quad (5)$$

By similar reasoning, we can obtain the density profile $\rho_m(t)$ for any segment m in the chain. With segment m fixed at position x, we suppose that a linear chain of m segments starting at x reaches within dx' of x', that $f-1$ chains of n segments are generated from x', and that a linear chain of $n-m$ segments is generated from x. The joint probability of success for these events is $[P_n(x')]^{f-1}P_m(x'|x)P_{m-n}(x)\,dx'$. Integration over x' then leads to the density profile for the mth segments. Replacing the discrete segment index with a continuous reduced variable $u = m/n$, we have the density profile $\rho(t,u)$ for segments at position u in subchains of n segments:

$$\rho(t,u) = \int_0^\infty [\mathrm{erf}(t')]^{f-1} \frac{1}{(\pi u)^{1/2}} [e^{-(t'-t)^2/u} - e^{-(t'+t)^2/u}] \mathrm{erf}\left(\frac{t}{(1-u)^{1/2}}\right) dt' \quad (6)$$

For $f = 1$, eqs 5 and 6 revert to integrals derived earlier[3] for linear chains. Thus, eq 6 gives

$$\rho(t,u) = \mathrm{erf}\left(\frac{t}{u^{1/2}}\right) \mathrm{erf}\left(\frac{t}{(1-u)^{1/2}}\right) \quad (7)$$

For the degenerate star with $f = 2$ (a linear chain of length $2n$), the integration in eq 6 can also be done analytically (see Appendix), leading to

$$\rho(t,u) = \mathrm{erf}\left(\frac{t}{(1+u)^{1/2}}\right) \mathrm{erf}\left(\frac{t}{(1-u)^{1/2}}\right) \quad (8)$$

Equations 7 and 8 necessarily constitute equivalent information, and one form can be translated directly into the other just by changing the way in which the segments of a linear chain are enumerated. For the general case $f > 2$, analytical integration of eqs 5 and 6 does not appear possible.

Characteristics of Chain Segment Density Profiles $\rho(t,u)$

Figures 1–4 illustrate comparisons among density profiles for linear chains and star–branched species with 4, 8, and 32 branches. Different measures of chain size are held fixed in each of the four sequences of curves, but the abscissas are scaled to represent the same measure of distances from the boundary. The density profile for the "branch node" (or middle segment) of the degenerate two-arm star is the same in all four graphs.

Figure 1 offers a comparison of density profiles for particular segments of linear and branched chains as branches of fixed length are added to the molecular model. The single curve for $f = 1$ is the profile for an end segment of a linear chain of n steps, as given by eq 2. The broken curve for $f = 2$ represents the density function $\rho_n(t) = \rho(t,1) = \mathrm{erf}(t/\sqrt{2})$ for an end segment of the two-arm star. Because of the doubled molecular weight, this linear chain is, on average, pushed farther away from the wall than the chain with $f = 1$. The solid curve for $f = 2$ is the profile of the middle segment. As

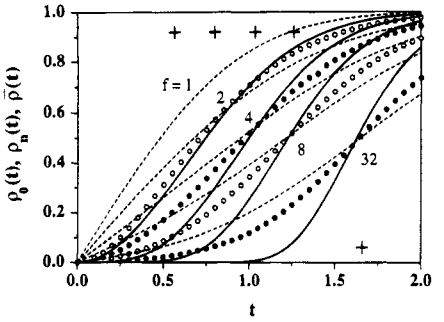

Figure 1. Segment density profiles for linear ($f = 1$, 2) and regular star ($f = 4$, 8, 32) chains in solution near a plane wall: free chain ends (dashed curves) and branch nodes (solid curves). The stars are all constructed from branches of the same length. The crosses in this and subsequent figures denote distances corresponding to half the mean projection for each molecule ($t = 1/\pi^{1/2}$, $(2/\pi)^{1/2}$, 1.0357, 1.2610, 1.6596 for $f = 1$, 2, 4, 8, 32, respectively). The circles mark the averaged segment density profiles $\bar{\rho}(t)$ for the branched species.

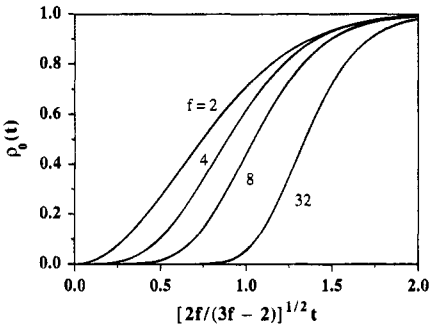

Figure 2. Segment density profiles of branch nodes for polymers with the same value of R_g and with f as indicated.

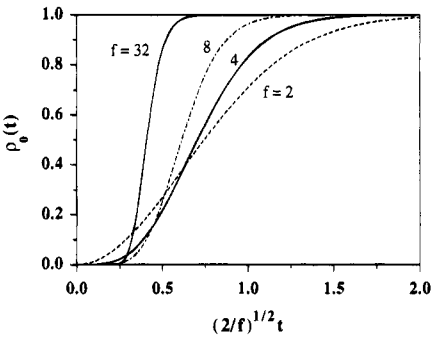

Figure 3. Segment density profiles of branch nodes for polymers with the same total number of segments $N = fn$ for f as indicated.

was pointed out in ref 3, the end-segment profile of this chain initially depends linearly on the distance from the wall while the initial dependence for the middle segment (or any interior segment) is quadratic. Thus, chain ends are favored relatively over interior segments as the total segment density approaches zero at the wall.

All the node profiles are sigmoidal, but the end-segment profiles for straight chains ($f = 1$, 2) exhibit no change in the sense of the curvature since these are just error functions. With increasing numbers of arms the end-segment profiles for stars assume an obviously sigmoidal shape.

For true branched molecules ($f = 4$, 8, 32 in Figure 1) the depletion layer thickens and the disparity between the end–segment profile and the node profile increases as the number of arms of the same mass is increased. It is easily confirmed for the free chain ends that the initial dependence of the profile on the reduced

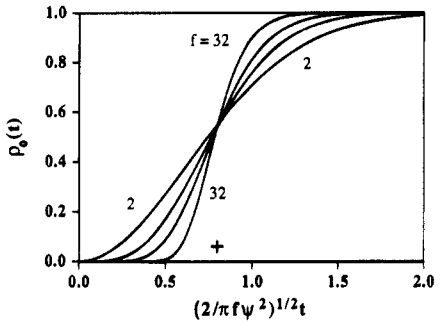

Figure 4. Segment density profiles of branch nodes for polymers with the same mean projection $\bar{X}$ for $f = 2, 4, 8, 32$.

distance remains linear, as the plots suggest, but the slope decreases with increasing f. Specifically, differentiation of eq 5 leads to

$$\lim_{t\to 0}\left[\frac{\partial\rho(t,1)}{\partial t}\right] = \frac{1}{\pi^{1/2}}\int_0^\infty [\mathrm{erf}(t')]^{f-1}\mathrm{e}^{-t'^2}\, 4t'\, \mathrm{d}t' \qquad (9)$$

For $f = 1$, 2, the right-hand side of eq 9 is $2/\pi^{1/2}$ and $(2/\pi)^{1/2}$, respectively. With the node density given by eq 4, it can be seen that $\rho_0(t)$ becomes proportional to t^f as $t \to 0$, and so the first $f - 1$ derivatives of $\rho_0(t) = \rho(t,0)$ vanish at the node limit $u = 1$.

The profiles for free ends and for nodes with $f > 2$ are singular cases, The general relation for any segment other than these is given by eq 6. The first derivative $\partial\rho(t,u)/\partial t$ vanishes as $t \to 0$, but the second remains finite:

$$\lim_{t\to 0}\left[\frac{\partial^2\rho(t,u)}{\partial t^2}\right] = \frac{16}{u^{3/2}(1-u)^{1/2}\pi}\int_0^\infty [\mathrm{erf}(t')]^{f-1}\mathrm{e}^{-t'^2/u}\, t'\, \mathrm{d}t' \qquad (10)$$

showing that $\rho(u,t)$ is initially a quadratic function of t, except for $u = 0$, 1, as it is for any interior segment of a linear chain.[3]

The asymptotic dependence at large t of the node density profile of the f-arm star,

$$1 - \rho(t,0) \approx f\,\mathrm{erfc}(t) \sim \frac{f\,\mathrm{e}^{-t^2}}{\pi^{1/2}t} \qquad (11)$$

is obtained by substituting the error function complement, $\mathrm{erfc}(t) = 1 - \mathrm{erf}(t)$, in eq 4, retaining the first two terms of the binomial expansion of $[1 - \mathrm{erfc}(t)]^f$ and introducing the asymptotic expansion for $\mathrm{erfc}(t)$. The asymptotic behavior for any u is also obtained similarly if $f \le 2$ from eq 7 or 8: thus, for the end segment of a degenerate star ($f = 2$), eq 8 leads to

$$1 - \rho(t,1) \sim \frac{2^{1/2}\mathrm{e}^{-t^2/2}}{\pi^{1/2}t} \qquad (12)$$

In Figure 2 we plot density profiles for branch nodes of molecules with different numbers of branches but the same root-mean-square radius of gyration R_g. If the repulsion effect near a wall is characterized by the overall size of the molecule, then R_g might be supposed to have some relevance as a structure-independent molecular parameter correlated with the thickness of the depletion layer. The mean–square radius for a star chain is

$$R_g^2 = \frac{nfb^2}{6}\left(\frac{3f-2}{f^2}\right) \qquad (13)$$

The second factor on the right–hand side is the ratio of mean–square radii of linear and regular-star chains of the same mass.[11] With A and the dimensionless distance t defined above, eq 13 is transformed to

$$R_g = \frac{1}{2A}\left(\frac{3f-2}{f}\right)^{1/2} \qquad (14)$$

and a dimensionless distance relative to R_g is

$$\frac{x}{2^{1/2}R_g} = 2^{1/2}t\left(\frac{f}{3f-2}\right)^{1/2} \qquad (15)$$

In Figure 2, $(\mathrm{erf}\, t)^f$ is plotted against $x/2^{1/2}R_g$ according to eq 15. The factor $2^{-1/2}$ scales the abscissa so that the curves for $f = 2$ in Figures 1 and 2 coincide. It is clear from the plot that stars with a given radius of gyration, but different numbers of arms, give node density profiles that are somewhat closer together than those for a series of stars with a common arm length, but the curves are still far from overlapping.

To obtain a comparison among stars with different numbers of branches but the same total mass, we note that A is proportional to $f^{1/2}$ if nf is held constant. It follows that the distance x from the wall is proportional to $t/f^{1/2}$ so that plotting $(\mathrm{erf}\, t)^f$ versus $(2/f)^{1/2}t$ gives the node profiles of different stars with the common distance coordinate adjusted to reproduce the profile for $f = 2$, as already indicated. Now the curves, shown in Figure 3, cross at short distances from the wall and then diverge markedly at greater distances.

A number of statistical measures of polymer chain dimensions besides R_g have been discussed for linear random-flight chains.[12] One that is of particular importance as a measure of the thickness of the depletion layer at a plane boundary is the average projection $\bar{X}$ of the *unconfined* molecule onto an axis.[12-16] It is easily demonstrated that the average thickness of the depletion layer is $\bar{X}/2$. That is, the total deficit of centers of mass of solute molecules in the depletion layer is the same as that associated with a step function with no centers of mass for a distance $\bar{X}/2$ from the wall and the concentration of the bulk solution phase at all greater distances.[15-17] It can also be shown that the equivalent segment-conserving step function for the density profile of any segment in a chain is at distance $\bar{X}/2$. Furthermore, this relation of the mean projection with the thickness of the depletion layer at a passive barrier holds for any molecular model, whether rigid or flexible,[15,17] in the absence of intermolecular interactions. Therefore, it must hold for random-flight stars, for which the mean projection is given by[2,15,16]

$$\bar{X} = (8nfb^2/3)^{1/2}\psi = 2f^{1/2}\psi/A \qquad (16)$$

where

$$\psi = \left(\frac{f}{\pi}\right)^{1/2}\int_0^\infty [\mathrm{erf}\, w^{1/2}]^{f-1}\mathrm{e}^{-w}\, \mathrm{d}w \qquad (17)$$

For $f = 1$, 2, eq 16 reduces to the results for linear chains of nf segments; for both cases, ψ is $\pi^{-1/2}$. Some values of the function ψ are tabulated in ref 2. The correspondence between eqs 9 and 17 should be noted.[18] It

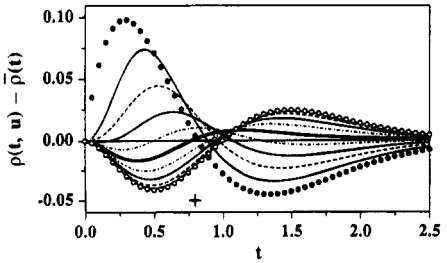

Figure 5. Deviation plots $[\rho(t,u) - \bar{\rho}(t)]$ vs t for degenerate star ($f = 2$): $u = 0$ (nodes, open circles), 0.1 (solid curve), 0.2 (dash curve), 0.3 (solid curve), 0.4 (dot–dash curve), 0.5 (bold curve), 0.6 (dot–dash curve), 0.7 (solid curve), 0.8 (dash curve), 0.9 (solid curve), 1.0 (free ends, filled circles).

follows that the initial slope of the end-segment profile with respect to t is $2\psi/f^{1/2} = A\bar{X}/f$.

Equation 16 suggests definition of another dimensionless length proportional to

$$\frac{2x}{\bar{X}} = \frac{t}{f^{1/2}\psi} \tag{18}$$

Plots of $(\mathrm{erf}\, t)^f$ versus $(2x/\bar{X})(2/\pi)^{1/2}$ in Figure 4 represent branch-node density profiles for a series of stars with a common $\bar{X}$ scaled so that the curve for $f = 2$ matches that in the preceding figures. The most prominent feature of this graph is the apparent common intersection of the node profiles where the abscissa value $(2/\pi)^{1/2} = 0.7979$ corresponds to $\bar{X}/2$. This might have been anticipated from what has been said above and from the centrally symmetrical disposition of the node in the star. More careful scrutiny, however, shows that this intuition is not quite correct. The curves do not actually meet at a common point. For f from 2 to 32, the node density at distance $\bar{X}/2$ from the boundary varies overall by only about 2%; it passes through a shallow minimum at $f = 7$. Had we compared end-segment profiles in the same way on the scale of Figure 4, a somewhat greater deviation of the curves from a common intersection would have been apparent. However, Figure 4 does illustrate the general significance of the mean projection as a measure of the thickness of the depletion layer: i.e., how the common value of $\bar{X}/2$ for the segment profiles corresponds to the same average thickness of the depletion layer. On the other hand, it is evident from inspection of Figure 2 that a common molecular radius of gyration among different branched species does not correlate with a common depletion layer thickness.

As the number of branches is increased and their length is decreased consistently with a fixed value of the mean projection, the molecules becomes more compact and the node density profiles become steeper, more closely resembling a step function. For an indefinitely large number of branches the curves in Figure 4 would asymptotically approach the step function for a hard sphere with radius equal to $\bar{X}/2$ of the chain with $f = 2$. The same trend can be seen in Figure 3 as branching is increased at fixed radius of gyration. The profile for free end segments of a given star species is always broader than that for the node, and thus the progressive steepening of the profiles with increasing f at fixed $\bar{X}$ (not shown) is less dramatic for chain ends.

In Figures 5–7, to illustrate on a magnified scale how density profiles vary with position u along a subchain as the number of branches in a star molecule is increased, we plot *differences* between $\rho(t,u)$ and the profile $\bar{\rho}(t)$ averaged over u (see below) versus t at 11

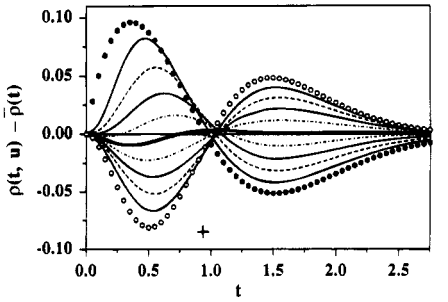

Figure 6. Deviation plots as in Figure 5, but for 3-arm star.

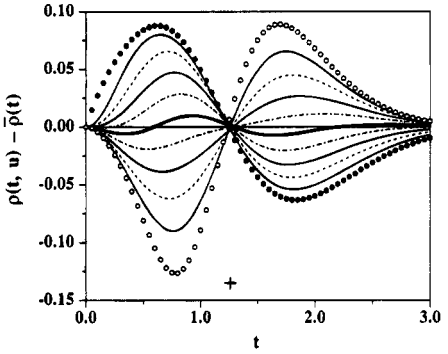

Figure 7. Deviation plots as in Figure 5, but for 8-arm star.

equally spaced values of u for a linear chain ($f = 2$) and for stars with three and eight branches.[19] The twisted surfaces in three dimensions depicted by the contours in each of these figures can be visualized as superimposed upon (or modulating) a $\bar{\rho}(t)$ surface that is sigmoidal in the t-direction and invariant along the u-coordinate. To facilitate comparison, the vertical scales are the same in the three figures. Comparing the plots, we see that the shape of the deviation plot for free chain ends is not much altered by addition of branches. Otherwise, as u decreases from unity, the effect of branches is to increase the magnitude of both negative and positive deviations for a given u (the positive and negative areas under a contour must be equal if all chain segments are to be accounted for). For the linear chain, the density profiles for $u = 0$, 0.1, 0.2 are hardly distinguishable on the scale of Figure 5. This is not unexpected since the "node" in this case does not mark a functional discontinuity.

The general trend at short distances from the wall, of deviations from $\bar{\rho}(t)$ that pass from negative at $u = 0$ to become progressively more positive with increasing u and reach a positive maximum at $u = 1$, indicates (as Figure 1 suggests) that the branch nodes are most strongly rejected from the wall, and the repulsion lessens the closer segments are to a free end along a chain contour. Figures 6 and 7 show, as already mentioned, that the difference in behavior between nodes and free ends is enhanced as more branches are introduced. It is evident from Figure 5 that density profiles for different parts of a linear chain do not intersect at a common point[3] (i.e., would not intersect a common horizontal line in a three-dimensional representation). Interestingly, though, the graphs for $f = 3$ and $f = 8$ suggest that as more branches are added, the set of profiles for each star species tend progressively toward a common intersection, perhaps at $t = A\bar{X}/2$, as the deviations from $\bar{\rho}(t)$ change sign. A plot of profiles like these for $f = 32$ (not shown) confirms the tendency toward a common intersection but the narrowed range

where the deviations change sign is slightly below $A\bar{X}/2$.

Overall Segment Density Profiles

It might be feasible in practice to label free chain ends or star nodes and study the distribution of labels near a boundary, but the overall segment density profile will usually be of greater interest in experimental studies. Thus it is pertinent to discuss

$$\bar{\rho}(t) = \int_0^1 \rho(t,u)\, du \tag{19}$$

the average of profiles $\rho(t,u)$ over segment positions u. Although the density profile for any chosen u (or m) is easily obtained by numerical integration of eq 6, accurate determination of $\bar{\rho}(t)$ requires more demanding two-dimensional numerical quadratures. Despite some convergence difficulties, the procedure was carried out successfully with the computer program Mathematica[20] (see Appendix). Results for a few branched species are listed in Table 1 and plotted in Figure 1, where the circles denote $\bar{\rho}(t)$ for $f = 2$, 4, 8, 32. Figures 5–7 show that no specific segment density profile coincides with $\bar{\rho}(t)$, but the profile for the middle segment of a subchain ($u = {}^1/_2$) perhaps matches most closely in all the plots shown. On the scale of Figure 1, the difference between $\bar{\rho}(t)$ and the middle-segment profile would scarcely be visible.

To obtain the limiting behavior of $\bar{\rho}(t)$ as $t \to 0$, we average the second derivative from eq 10 over the segment position variable u. The double integral is evaluated analytically by doing the integration with respect to u first:

$$\int_{u=0}^{1} \lim_{t\to 0}\left[\frac{\partial^2 \rho(t)}{\partial t^2}\right] du = \frac{16}{\pi}\int_{t'=0}^{\infty}\int_{u=0}^{1} [\mathrm{erf}(t')]^{f-1} t' \frac{e^{-t'^2/u}}{u^{3/2}(1-u)^{1/2}}\, du\, dt' = \frac{16}{\pi^{1/2}}\int_0^{\infty} [\mathrm{erf}(t')]^{f-1} e^{-t'^2}\, dt' = \frac{8}{f} \tag{20}$$

It follows that $\bar{\rho}(t)$ tends to zero as $(4/f)t^2$.

Starting from eq 7 or 8, it is not difficult to obtain the asymptotic behavior of $\bar{\rho}(t)$ for linear chains ($f = 1$, 2). The derivation for the latter case, shown in the Appendix, gives

$$1 - \bar{\rho}(t) \sim \frac{e^{-t^2/2}}{\pi^{1/2}} \frac{4(2^{1/2})}{t^3} \tag{21}$$

The corresponding expression for $f = 1$ is recovered by replacing t with $2^{1/2}t$.[21]

Using a mean-field model of the depletion layer for linear polymer chains at a plane boundary, Joanny et al.[22] obtained a segment density profile that Allain et al.[5] later showed can be expressed by the square of a hyperbolic tangent: i.e.

$$\rho'(t) = \tanh^2(\beta t) \tag{22}$$

in terms of our variables, with β an adjustable parameter.[23] Thus it is of interest to inquire how well this relation agrees with the averaged density profiles we have derived. In fitting any $\bar{\rho}(t)$, we do not regard the power 2 as adjustable since it is mandatory if the quadratic behavior of $\bar{\rho}(t)$ as $t \to 0$ is to be preserved.

Table 1. Averaged Segment Density Profiles $\bar{\rho}(t)$ for Linear and Star-Branched Random-Flight Chains

t	$f = 2$	$f = 3$	$f = 4$	$f = 8$	$f = 12$
0.00	0	0	0	0	0
0.05	0.004801	0.003183	0.002377	0.001176	0.000780
0.10	0.018408	0.012176	0.009061	0.004448	0.002937
0.15	0.039644	0.026241	0.019486	0.009510	0.006261
0.20	0.067360	0.044745	0.033210	0.016154	0.010619
0.25	0.10045	0.067147	0.049896	0.024253	0.015941
0.30	0.13786	0.092967	0.069291	0.033750	0.022207
0.35	0.17860	0.12178	0.091200	0.044645	0.029441
0.40	0.22177	0.15317	0.11546	0.056984	0.037701
0.45	0.26652	0.18677	0.14194	0.070844	0.047073
0.50	0.31212	0.22220	0.17047	0.086326	0.057666
0.55	0.35790	0.25908	0.20090	0.10354	0.069603
0.60	0.40330	0.29704	0.23303	0.12259	0.083021
0.65	0.44781	0.33572	0.26664	0.14357	0.098062
0.70	0.49105	0.37476	0.30147	0.16654	0.11487
0.75	0.53269	0.41382	0.33726	0.19151	0.13356
0.80	0.57247	0.45256	0.37370	0.21846	0.15425
0.85	0.61021	0.49069	0.41048	0.24731	0.17701
0.90	0.64578	0.52793	0.44731	0.27791	0.20187
0.95	0.67911	0.56405	0.48387	0.31007	0.22880
1.00	0.71018	0.59883	0.51989	0.34354	0.25772
1.05	0.73898	0.63213	0.55511	0.37804	0.28848
1.10	0.76557	0.66380	0.58929	0.41327	0.32087
1.15	0.78999	0.69375	0.62224	0.44888	0.35462
1.20	0.81235	0.72191	0.65379	0.48456	0.38944
1.25	0.83273	0.74827	0.68381	0.51999	0.42499
1.30	0.85125	0.77282	0.71222	0.55486	0.46091
1.35	0.86802	0.79557	0.73894	0.58889	0.49687
1.40	0.88316	0.81657	0.76394	0.62186	0.53250
1.45	0.89679	0.83586	0.78722	0.65355	0.56751
1.50	0.90902	0.85353	0.80879	0.68380	0.60161
1.55	0.91997	0.86964	0.82869	0.71249	0.63454
1.60	0.92974	0.88428	0.84696	0.73953	0.66612
1.65	0.93845	0.89754	0.86368	0.76486	0.69616
1.70	0.94618	0.90951	0.87891	0.78845	0.72456
1.75	0.95304	0.92028	0.89274	0.81031	0.75124
1.80	0.95910	0.92994	0.90524	0.83047	0.77613
1.85	0.96445	0.93857	0.91651	0.84897	0.79925
1.90	0.96916	0.94628	0.92663	0.86587	0.82059
1.95	0.97330	0.95313	0.93570	0.88124	0.84019
2.00	0.97693	0.95920	0.94379	0.89516	0.85811
2.05	0.98011	0.96457	0.95098	0.90773	0.87442
2.10	0.98288	0.96930	0.95736	0.91902	0.88920
2.15	0.98529	0.97347	0.96301	0.92913	0.90254
2.20	0.98739	0.97712	0.96799	0.93816	0.91453
2.25	0.98921	0.98031	0.97236	0.94618	0.92526
2.30	0.99079	0.98310	0.97620	0.95329	0.93484
2.35	0.99215	0.98553	0.97955	0.95957	0.94334
2.40	0.99333	0.98763	0.98247	0.96510	0.95088
2.45	0.99434	0.98946	0.98501	0.96995	0.95753
2.50	0.99520	0.99103	0.98722	0.97420	0.96339
2.55	0.99595	0.99239	0.98912	0.97790	0.96852
2.60	0.99658	0.99355	0.99077	0.98113	0.97300
2.65	0.99712	0.99456	0.99218	0.98392	0.97691
2.70	0.99758	0.99541	0.99339	0.98634	0.98031
2.75	0.99797	0.99614	0.99443	0.98842	0.98325
2.80	0.99830	0.99676	0.99532	0.99021	0.98579
2.85	0.99858	0.99729	0.99607	0.99174	0.98797
2.90	0.99882	0.99773	0.99671	0.99305	0.98985
2.95	0.99902	0.99811	0.99725	0.99417	0.99146
3.00	0.99919	0.99843	0.99771	0.99512	0.99283

To fix the value of β, the most appropriate criterion is probably to require that the mean thickness of the depletion layer defined by $\tanh^2(\beta t)$ match that for the correct random-flight profile. To obtain the value of β subject to this condition, we recall that the total segment deficit in the depletion layer is represented on a plot of $\bar{\rho}(t)$ versus t by the area between the curve and the horizontal line $\rho = 1$. Accordingly, with the fitting

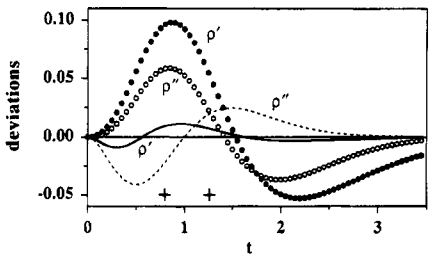

Figure 8. Deviations from $\bar{\rho}(t)$ plotted for two approximation functions $\rho'(t)$ and $\rho''(t)$ for linear chain with $f = 2$ (curves) and for 8-arm star (circles).

function, we must have

$$\int_0^\infty [1 - \tanh^2(\beta t)]\, dt = 1/\beta \qquad (23)$$

Because the height of the normalized step function representing the depletion layer is unity, the integral is numerically equal to the value of t corresponding to the depletion layer thickness. Hence for linear chains we set β equal to $\pi^{1/2}$ ($f = 1$) or $(\pi/2)^{1/2}$ ($f = 2$) to obtain the desired $\rho'(t)$ function.

Since the deviation of $\rho'(t)$ from $\bar{\rho}(t)$ for a linear chain is barely discernible on the scale of the plots in Figures 1–4, we have plotted the differences $[\rho'(t) - \bar{\rho}(t)]$ on an expanded ordinate scale in Figure 8. The absolute deviations are quite small everywhere, but they do become large in percentage terms when $\bar{\rho}(t)$ is itself small (the limit of $\rho'(t)/\bar{\rho}(t)$ as $t \to 0$ is 0.785).

The fit with eq 23 and the circumstance that $\bar{\rho}(t)$ for a linear chain is an average of products of two error functions prompt a further question as to the possibility of fitting $\bar{\rho}$(t) with the square of a single error function that gives the correct depletion layer thickness. The appropriate function has the form

$$\rho''(t) = [\mathrm{erf}(\alpha t)]^2 \qquad (24)$$

and by reasoning analogous to that leading to eq 23, we have

$$\int_0^\infty [1 - \mathrm{erf}^2(\alpha t)]\, dt = \frac{1}{\alpha}\left(\frac{2}{\pi}\right)^{1/2} \qquad (25)$$

We set the right-hand side equal to the depletion layer thickness, as before, and solve for the parameter α. The result, shown in Figure 8, is a less satisfactory approximation to $\bar{\rho}(t)$ than the hyperbolic tangent function.

We can apply these arguments in fitting the forms of ρ' and ρ'' to segment density profiles of regular stars, for which the depletion layer thickness corresponds to $t = f^{1/2}\psi$. Then, matching the layer thickness requires values for the parameters: $\beta = (f^{1/2}\psi)^{-1}$ and $\alpha = (2\pi^{1/2}\psi)^{-1}$. The corresponding deviations from $\bar{\rho}(t)$ for the eight-arm star ($\psi = 0.445842$) are plotted in Figure 8. It is evident that with introduction of branching the overall fit to $\bar{\rho}(t)$ is much worse than in the linear-chain case for both $\rho'(t)$ and $\rho''(t)$, though $\rho''(t)$ is now a better fit than $\rho'(t)$.

Summary

Equilibrium distributions of dissolved regular-star branched molecules near an impenetrable plane boundary have been calculated according to random-flight statistics. In keeping with what was found earlier for linear chains, interior segments of the molecule are more strongly repelled from the barrier than free chain ends. The additional structural feature, the branch node, is still more strongly repelled. As the segment density increases from zero at the barrier, the initial dependence of the segment density profiles on distance t is quadratic except for the singular cases of free ends and nodes, for which the densities are, respectively, proportional to t and to t^f. Except for linear-chain ends, the profiles are sigmoidal and become progressively steeper in going from a free end to the node. Except for linear-chain ends and branch nodes, individual segment profiles are expressed by integrals that must be evaluated numerically. Determination of the averaged density profile $\bar{\rho}(t)$ for a star species thus requires double numerical integration, which has been accomplished after taking due regard for the pathology of the integrand at the limits of a chain end or node. Although, as is required on general principles, different stars with the same value of the mean molecular projection on a line give the same average thickness of the depletion layer at a plane barrier, neither their averaged density profiles $\bar{\rho}(t)$ nor the $\rho(t,u)$ for individual segments superpose since the sigmoidal profiles become steeper as the branch functionality f increases.

The segment density profiles derived here for the "one-wall" case obviously represent asymptotic limits for star polymers confined to slab-shaped cavities between parallel infinite planes when the distance between plates is much greater than chain dimensions.

The random-flight chain is a physically realistic model only under near-Θ conditions; but it must be noted that there is evidence that star molecules may deviate from random-flight statistics even at the Θ temperature.

Appendix: Mathematical Details

Integration of Eq 5 for $f = 2$. For the degenerate star with $f = 2$ (a linear chain of $2n$ segments), eq 5 becomes

$$I = \frac{1}{\pi^{1/2}}\int_0^\infty \mathrm{erf}(t')[e^{-(t'-t)^2} - e^{-(t'+t)^2}]\, dt' \qquad (A1)$$

We introduce the error function complement, erfc(t′) = 1 − erf(t′) and write, according to eq 2

$$I = \mathrm{erf}(t) - I_2 \qquad (A2)$$

$$I_2 = \frac{1}{\pi^{1/2}}\int_0^\infty \mathrm{erfc}(t')[e^{-(t'-t)^2} - e^{-(t'+t)^2}]\, dt' \qquad (A3)$$

The integral I_2 may be transformed into

$$I_2 = \frac{2}{\pi}\int_0^\infty \int_0^\infty \mathrm{erfc}(t')\sin(\alpha t')\sin(\alpha t)\, e^{-\alpha^2/4}\, dt'\, d\alpha \qquad (A4)$$

a result that can be obtained from Fourier's integral theorem.[10] The integration over t' gives

$$I_2 = \frac{2}{\pi}\int_0^\infty \sin(\alpha t)[e^{-\alpha^2/4} - e^{-\alpha^2/2}]\frac{d\alpha}{\alpha} \qquad (A5)$$

The two integrals in this expression are representations of error functions:

$$I_2 = \mathrm{erf}(t) - \mathrm{erf}(t/2^{1/2}) \qquad (A6)$$

so that, finally, we have

$$I = \mathrm{erf}(t/2^{1/2}) \qquad (A7)$$

The integrations over t' and α are given by standard

forms.[24] As required, the result for I is just that obtained directly from eq 2 for an end segment of a linear chain of $N = 2n$ segments:

$$\rho = \mathrm{erf}\left[\left(\frac{3}{2Nb^2}\right)^{1/2} x\right] = \mathrm{erf}\left(\frac{t}{2^{1/2}}\right) \qquad \text{(A8)}$$

This correspondence incidentally verifies the catenation of probabilities that is the basis of eqs 5 and 6. A derivation like this one, starting with eq 6 and $f = 2$, must lead to recovery of the density profile $\rho(t,u)$ of eq 8.

Integrations in Two Dimensions. For numerical integration, Mathematica (Version 2.1) utilizes Gauss quadratures.[20] On the Macintosh Quadra 700 computer used in this work, the range of integration in one dimension is divided initially into six subdivisions according to the Gauss formula. Recursive bisections of the intervals are used for successive integrations in attempting to realize the precision goal of ten digits less than machine precision: i.e., 19 − 10 = 9.

Without care to circumvent the pathology of the integrand, attempts at two-dimensional integration of $\rho(t,u)$ according to eqs 6 and 19 were usually attended by error and/or warning messages. At fixed u, the integrand of eq 6 exhibits a single peak as a function of t' and tends to zero away from the peak. For most of the range of u, the peak is broad and does not change rapidly as u is varied. However, as u becomes very small, the peak quickly narrows, approaching the limit of infinite height and zero width as $u \to 0$ and $t' = t$. Depending on parameters f and t, the integration failed to converge or converged to a value that was too small, indicating that a portion of the integrand had been missed. Convergence was achieved by doing the integration piecewise, dividing the infinite integration range for t' into four regions with partitions at $t' - 0.01$, t', and $t' + 0.01$. With the singularity at a range boundary, the computation converged properly (Mathematica looks for singularities at endpoints). The approach to the limit $u \to 1$ elicited messages warning of numerical overflow. This difficulty was avoided, without compromising results recorded to six significant figures, by setting the upper limit for u short of unity by an increment of 10^{-7} or 10^{-8}. Selected results were checked by changing the subdivisions of the t range near t' or increasing the maximum number of recursions (default 6) in the integration.

Asymptotic Dependence of $\bar{\rho}(t)$. To obtain the asymptotic behavior of $\bar{\rho}(t)$ for a linear chain ($f = 2$), we substitute the error function complement into eq 8, expand the product, and drop the term containing a product of erfc functions because it ultimately would contribute only an asymptotic dependence of higher order than the terms we retain:

$$1 - \bar{\rho}(t) \approx \int_0^1 \mathrm{erfc}\left(\frac{t}{(1+u)^{1/2}}\right) du + \int_0^1 \mathrm{erfc}\left(\frac{t}{(1-u)^{1/2}}\right) du = \int_1^2 \mathrm{erfc}\left(\frac{t}{u^{1/2}}\right) du + \int_0^1 \mathrm{erfc}\left(\frac{t}{u^{1/2}}\right) du = \int_0^2 \mathrm{erfc}\left(\frac{t}{u^{1/2}}\right) du \qquad \text{(A9)}$$

The substitution $x = 1/u^{1/2}$ and an integration by parts lead to

$$1 - \bar{\rho}(t) \approx 2\int_{1/2^{1/2}}^{\infty} \frac{\mathrm{erfc}(tx)}{x^3}\, dx = 2\,\mathrm{erfc}\left(\frac{t}{2^{1/2}}\right) - \frac{2t}{\pi^{1/2}} \int_{1/2^{1/2}}^{\infty} \frac{e^{-t^2x^2}}{x^2}\, dx \qquad \text{(A10)}$$

The last integral is in a standard form[25] giving

$$1 - \bar{\rho}(t) \approx 2\,\mathrm{erfc}\left(\frac{t}{2^{1/2}}\right) - \frac{2t}{\pi^{1/2}}\left[2^{1/2} e^{-t^2/2} - \pi^{1/2} t\,\mathrm{erfc}\left(\frac{t}{2^{1/2}}\right)\right] \qquad \text{(A11)}$$

If the erfc function is replaced by the asymptotic series

$$\mathrm{erfc}(x) \sim \frac{e^{-x^2}}{\pi^{1/2} x}\left(1 - \frac{1}{2x^2} + \frac{1\cdot 3}{2^2x^4} - \frac{1\cdot 3\cdot 5}{2^3x^6} + \ldots\right) \qquad \text{(A12)}$$

cancellation of terms leaves eq 21 as the limiting behavior. Regardless of the validity of the final manipulations of individual terms of a nonconvergent series, the important aspect of eqs 21 and A11 is the dependence on $\exp(-t^2/2)$.

To work out the general case for $f \geq 2$, we express eq 6 in terms of erfc functions, expand $(1 - \mathrm{erfc}\ t')^{f-1}$, multiply out factors containing erfc, and drop terms containing products of erfc functions. Then, integrations over t' are effected via transformations like those in eqs A1 to A7. With these results written in terms of erfc functions, averaging over u involves integration by parts, as in eq A10. The asymptotic contribution to $1 - \bar{\rho}(t)$ turns out to be just the right-hand side of eq A11 multiplied by $f - 1$. Therefore, with branch length held constant, $1 - \bar{\rho}(t)$ is asymptotically proportional to $f - 1$.

References and Notes

(1) Asakura, S.; Oosawa, F. *J. Chem. Phys.* **1954**, *22*, 1255.
(2) Casassa, E. F.; Tagami, Y. *Macromolecules* **1969**, *2*, 14.
(3) Casassa, E. F. *Macromolecules* **1984**, *17*, 601.
(4) Yang, S.-I.; Sperling, L. S.; Casassa, E. F. *Macromolecules* **1990**, *23*, 4582.
(5) Allain, G.; Ausserre, C.; Rondelez, F. *Phys. Rev. Lett.* **1982**, *49*, 1694.
(6) Caucheteux, I.; Hervet, H.; Jerome, R.; Rondelez, F. *J. Chem. Soc., Faraday Trans.* **1990**, *68*, 1369.
(7) Kent, M. S.; Bosio, L.; Rondelez, F. *Macromolecules* **1992**, *25*, 6231.
(8) Feigin, R. I.; Napper, D. H. *J. Colloid Interface Sci.* **1980**, *74*, 567; **1980**, *75*, 525.
(9) It will be recognized that the expression for $P_n(x'|x)$ is formally equivalent to that for the temperature distribution in a one-dimensional solid (e.g., a long rod) at a time n after introduction of an instantaneous heat source at distance x from an end in contact with a heat sink at zero temperature. In the language of heat flow, eq 1 is a solution of the "diffusion" equation with an "absorbing" boundary. That the absorbing boundary is the correct constraint was definitively established after some controversy [see Di Marzio, E. A. *J. Chem. Phys.* **1965**, *42*, 2102].
(10) Carslaw, H. S.; Jaeger, J. C. *Conduction of Heat in Solids*, 2nd ed.; Oxford University Press: London, 1959. This is a classic treatise on heat conduction under boundary conditions. In the present context, see especially Chapter 2.
(11) Zimm, B. H.; Stockmayer, W. H. *J. Chem. Phys.* **1949**, *17*, 1301.
(12) Volkenstein, M. V. *Conformational Statistics of Polymeric Chains*; Wiley-Interscience: New York, 1963; Chapter 4.
(13) Precisely, X is defined as the maximum distance between parallel planes perpendicular to a given axis that both intersect the instantaneous chain configuration. $\bar{X}$ must not be confused with Volkenstein's "mean cross-sectional dimension $\bar{Q}$, which is averaged differently. Some earlier discus-

sions of the projection of the linear random-flight chain and its distribution are cited in refs 3 and 15.
(14) van Kreveld, M. E. *J. Polym. Sci., Polym. Phys. Ed.* **1975**, *13*, 2253.
(15) Casassa, E. F. *Macromolecules* **1976**, *9*, 182.
(16) Casassa, E. F. *J. Polym. Sci., Polym. Symp.* **1985**, *72*, 151.
(17) Giddings, J. C.; Kucera, E.; Russell, C. P.; Myers, M. N. *J. Phys. Chem.* **1968**, *72*, 4397. These authors derive $\bar{X}$, which they call the mean external diameter, for rigid molecular models.
(18) Transcription of eq 15 has been plagued by errors. In ref 14, e^{-w} is rendered as e^{-2}; and the defining equation in ref 2 has an extra factor $f^{1/2}$. An alternative form given by the unnumbered equation following eq A12 in ref 2 is correct, even though eq A12 itself has misplaced parentheses.
(19) Other representations of the $\rho(t,u)$ geometrical surface for a linear chain are given in refs 3 and 16.
(20) Wolfram, S. *Mathematica,* 2nd ed.; Addison–Wesley: Redwood City, CA, 1991; pp 683–686, 830.
(21) The asymptotic formula, $1 - \bar{\rho}(t) \sim 2 \exp(-t^2)/\pi^{1/2}t^3$ for the linear chain with $f = 1$ is given incorrectly in ref 3.
(22) Joanny, J. F.; Leibler, L.; de Gennes, P.-G. *J. Polym. Sci., Polym. Phys. Ed.* **1979,** *17*, 1073.
(23) Equation 2.19 in ref 22 leads to eq 22 here, only if an error is corrected: the last term on the right hand side should read $v\psi_0^2(\psi^2 - \psi_1^2)$. The correct derivation is given in de Gennes's book [de Gennes, P.-G. *Scaling Concepts in Polymer Physics*; Cornell University Press: Ithaca, NY, 1979; Chapter 9].
(24) Gradshteyn, I. S.; Ryzhik, I. M. *Tables of Integrals, Series, and Products: Corrected and Enlarged Edition*; Academic Press: New York, 1980. See integrals 6.311 and 3.952.6. These integrals bear the same designations in the Fourth Edition, 1965.
(25) See ref 24: 3.461.5.

MA950440O